Mechanical resonance characteristics of a cylindrical semiconductor heterostructure containing a high-mobility two-dimensional electron gas

H. Okamoto,[1] W. Izumida,[2] Y. Hirayama,[2,3,4] H. Yamaguchi,[1] A. Riedel,[5] and K.-J. Friedland[4,5,*]

[1]*NTT Basic Research Laboratories, 3-1 Morinosato Wakamiya, Atsugi-shi, Kanagawa 243-0198, Japan*

[2]*Department of Physics, Tohoku University, Aramaki, Aoba, Sendai, Miyagi 980-8578, Japan*

[3]*ERATO Nuclear Spin Electronics Project, Aramaki, Aoba, Sendai, Miyagi 980-8578, Japan*

[4]*WPI-AIMR, Tohoku University, Katahira, Aoba, Sendai, Miyagi 980-8577, Japan*

[5]*Paul-Drude-Institut für Festkörperelektronik, Hausvogteiplatz 5–7, 10117 Berlin, Germany*

(Received 27 December 2013; revised manuscript received 22 May 2014; published 6 June 2014)

We investigate the mechanical resonance characteristics of semiconductor rolled-up tubes containing a high-mobility two-dimensional electron gas (HM2DEG) by optical and electrical means. The observed mode frequencies are in an excellent agreement with the theoretically calculated frequencies for the ground bending and excited bending and axial modes. The effect of the curvature is to increase the frequencies of the ground bending modes and the axial wave modes, while decreasing the frequencies of the first excited bending modes. We find significant splitting of the bending and twisting modes by the residual stress effects due to axial shear relaxation in z-dependent modes. The HM2DEG interacts with the mechanical motion due to Eddy currents and embedded impedances. A prominent asymmetry appears in the vibration amplitude with respect to the direction of the magnetic field. This originates from the broken symmetry of the HM2DEG on the curved surfaces.

DOI: 10.1103/PhysRevB.89.245304 PACS number(s): 62.25.Jk, 68.65.Ac, 72.50.+b, 73.50.Rb

I. INTRODUCTION

The self-rolling of thin strained semiconductor bilayer systems as proposed by Prinz and coworkers [1] became now an important method for the fabrication of free-standing semiconductor structures. The fabrication of the strained semiconductor bilayer systems is based on pseudo morphologically epitaxial heterostructures grown by molecular-beam epitaxy. Semiconductor rolled-up tubes (SRTs) allow for new functionalities in micro- (MEMS) and nanoelectromechanical systems (NEMS) [2–5]. One of the outstanding advantages of SRT is that the curvature enables the stabilization of the shape [6], making them an ideal system when thin but large-area cantilevers are required. However, there are only few studies on vibration properties of rolled-up systems, while the SRTs represent now an inimitable system to study physical properties in a nontrivial topology. A new class of unique physical experiments and also functionality of MEMS and NEMS rose up with the possibility to fabricate two-dimensional high-mobility electron gases (HM2DEG) in thin free-standing semiconductor structures. In particular, using a specific heterojunction, where the HM2DEG in a 13-nm-wide GaAs single quantum well is effectively protected from charged surface states, the electron mobility in the quantum well remains high even after fabrication of free-standing layers [7] and, particularly, in SRTs with a layer thickness of less than 170 nm [8,9]. Implementing this new design, the low-temperature mean free path of electrons l_S can be kept comparable to the curvature radius r of the tube, opening the way to investigate curvature-related adiabatic motion of electrons on a cylindrical surface, such as trochoid- or snakelike trajectories [8,10]. Placing an SRT with an HM2DEG in a static and homogeneous magnetic field $\mathbf{B}_0$, the fundamental dominant modification is the gradual change of the component of the magnetic field perpendicular to the surface $B_\perp$ along the periphery of the tube, which is equivalent to a gradual change of the filling factor ν with far reaching consequences for the quantum Hall effect in a curved space [11].

The combination of free-standing semiconductor layers with an HM2DEG represents an excellent opportunity to enhance the functionality of MEMS and NEMS. Therefore the characteristics of nanoscale mechanical resonators recently attracted much attention and have been studied by many world-wide leading groups. In thicker free-standing planar cantilever structures, the HM2DEG was used as force and displacement sensors based on transport measurements [12,13] and also as tools for measuring semiconductor electronic properties such as the magnetization [14–16]. For small and low mass mechanical resonators, one of the most important targets is to study the quantum-mechanical properties of macroscopic objects as shown, for example, in Refs. [17] and [18]. The cylindrical semiconductor heterostructure is a promising candidate that meets these requirements so that the study of mechanical oscillation characteristics is undoubtedly important and promising to advance the study of not only semiconductor physics but also the quantum physics concerning macroscopic objects. In addition, the multimode vibration has recently been studied much more in detail as the enhanced nonlinearities in such tiny mechanical objects can mix different modes, enabling controlled coherent oscillation, phonon-lasing operation, and even the two-mode thermal and quantum noise squeezing [19–21], whereby the mechanism, which induces the mixing of different normal modes, plays an essential role and could be clarified by an accurate theoretical framework [22]. Therefore the detailed and accurate understanding of multimode vibration in this rolled structure leads to high impact both on classical and quantum nonlinear physics. The dynamic backaction induced by the electron motion enables not only the frequency and amplitude of the vibration modes to be changed, but also the

*Corresponding author: kjf@pdi-berlin.de

mechanical vibration to be dynamically amplified or cooled to study the quantum-mechanical behavior of mechanical systems [17,18,23,24]. Micromechanical cantilevers with an integrated two-dimensional electron system were shown to be extremely sensitive to small strain in the detection of localized-delocalized transition of electronic states. The appearance of a magneto-piezovoltage may exert friction on the mechanical vibrations [28,29].

Here, we will investigate the SRT as mechanical resonators constituted as vibrating cylindrically rolled-up cantilever shells of rectangular planform that are clamped along one straight edge and are free on the other three edges. The modeling of these systems by both numerical and analytical methods showed a clear impact of the curvature on the frequencies of the fundamental flexural modes [25]. In addition, we will demonstrate that the implemented HM2DEG can be used to excite and detect mechanical vibration in order to use SRT as MEMS or NEMS with a high application functionality. The interaction of the mechanical motion of the resonator with the embedded HM2DEG is of particular interest. It was already demonstrated that the magnetomotive excitation and detection in double-clamped cantilever structures with implemented conducting stripes exhibit backaction of the excited electromagnetic forces (emf) onto the mechanical properties [27]. We will demonstrate that the particular mechanical-electrical interaction shows clear signature of the curved HM2DEG, like asymmetries in a homogeneous magnetic field, which will open additional functionalities in the application of curved cantilevers.

II. EXPERIMENTAL

The layer stack, with an overall thickness of 170 nm including the high-mobility 2DEG, was grown by molecular-beam epitaxy on top of a 20-nm-thick $In_{0.15}Ga_{0.85}As$ stressor layer, an essential component of the strained multilayered films (SMLF). An additional 50-nm-thick AlAs sacrificial layer is introduced below the SMLF in order to separate the SMLF from the substrate. The SMLF were released by selective etching from the sacrificial AlAs layer with a 5% HF acid/water solution at 4 °C starting from a [100] edge. In order to relax the strain, the SMLF rolls up along the [010] direction forming a tube with a radius r of about 20 μm. As a function of the release-layer etching time, the length l_y along the circumference of the SRT varies. We define a pitch factor $p = l_y/(2\pi r)$, which, in fact, is the winding number. Here, we use SRT with $p \leqslant 1$. Consequently, the SRT represents a curved cantilever with an open end that ideally does not touch the opposite wafer surface. The length of the SRT along the cylinder axis is as large as $l_x = 1.3$ mm, which constitutes a cantilever with an area as large as 0.16 mm^2. For the optical investigation of the mechanical motion, we mounted the device onto a piezoceramic actuator [PZT: $Pb(Zr,Ti)O_3$] to excite out-of-plane mechanical vibrations. To identify each vibration mode of the SRT, we investigated the vibration amplitudes $z_{\rm rms}$, (rms is a root mean square) as a function of the positions along the axial direction (x) and frequencies (f). This was carried out with He:Ne laser Doppler interferometry in vacuum (1.5×10^{-4} Pa) at room temperature, while the SRT was actuated by applying an alternating voltage, $V_{\rm ac}(f) = 0.1V_{\rm rms}$, to the PZT.

For the electrical excitation and detection of the mechanical vibrations, we use SRTs with lithographically designed electronic structures in the 2DEG. We report on specific heterostructures that are described in Refs. [8] and [11] and which have a carrier density of $n \cong (6.8\text{–}7.2)\times10^{15}$ m^{-2} and a mobility of up to 90 m^2 V^{-1} s^{-1} along the [100] crystal direction before and after rolling-up. The electronic structure contains conducting paths (CP), which are formed by 2-μm-wide and about 60-nm-deep shallow-etched trenches in the 2DEG. Any pair of CP defines a loop on the SRT, ending at the Ohmic contact pads on the flat part of the wafer. The CP lead along the axial direction of the cylinder with a length up to $l_{\rm CP} \leqslant 600$ μm, see inset in Fig. 5, which shows two close loops schematically. In a magnetic field $\mathbf{B}_0$ and by actuating the SRT with an ac current I along one CP loop, we measure an emf voltage at another CP contact pair by a lock-in amplifier. With this configuration, which is similar to a four-terminal measurement in the usual magneto-transport experiments, we can control the distance between the exciting and measuring loops, thereby minimizing the cross-talk signals. Alternatively, the SRT may be actuated by applying an ac-voltage to the PZT and measuring the emf at any of the CP pairs.

III. RESULTS AND DISCUSSION

A. Optical detection of fundamental oscillations of rolled-up heterostructure

For the optical investigation of the mechanical motion, we use SRTs, which do not contain any electronic structure in the 2DEG, see Fig. 1(c). Figure 2 shows the dependence of the vibration amplitudes $z_{\rm rms}$ as a function of frequencies and positions x in the axial direction of the SRT. In the frequency region from 5–80 kHz, we observe five modes, which resonance frequencies we assign to the ground and first excited bending modes $f_1^{(\rm b)}, f_2^{(\rm b)}$, the ground and first excited twisting modes $f_1^{(\rm t)}$ and $f_2^{(\rm t)}$ and the axial mode $f_1^{(\rm a)}$ according to Ref. [25], and which we recalculated by taking into account the actual parameters of the SRT. As expected, the bending modes $f_1^{(\rm b)} = 26.0$ kHz and $f_2^{(\rm b)} = 57.5$ kHz do not show any node in the $z_{\rm rms}(x)$ dependence along the axial axis, while the twisting modes $f_1^{(\rm t)} = 31.5$ kHz and $f_2^{(\rm t)} = 64.5$ kHz obey one node with maximum vibration amplitudes at both ends of the tube. Accordingly, we ascribe the two doublets around 30 kHz (mode 1, mode 2) and 60 kHz (mode 3, mode 4) as the ground and first excited modes, respectively, consisting each of a bending and a twisting mode. The mode 5 at 68 kHz is the single axial mode. At even higher frequencies we find a manifold of other modes (not shown in Fig. 2), where the two prominent modes at 168 and 186 kHz (mode 6, mode 7) both show nodes in the axis direction may be a first excited axial wave of two nodes and a second excited twisting mode coupled to an axial wave of 5 nodes, respectively. The first excited axial mode $f_1^{(\rm a)}$ at 71.8 kHz develops a clear node pattern along the axial direction with two nodes. Note that the frequency of the fundamental bending mode $f_1^{(\rm b)}$ is larger by a factor of 1.54 as compared with the fundamental eigenfrequency of the bending mode for a wide and flat cantilever plate $f_1^{(0)} = h/2\pi(\lambda_1^{(0)}/l_y)^2\sqrt{E/[12(1-\nu^2)\varrho]} = 16.9$ kHz, where l_y is the length, h is the thickness of the cantilever, $\lambda_1^{(0)} = 1.875$, and

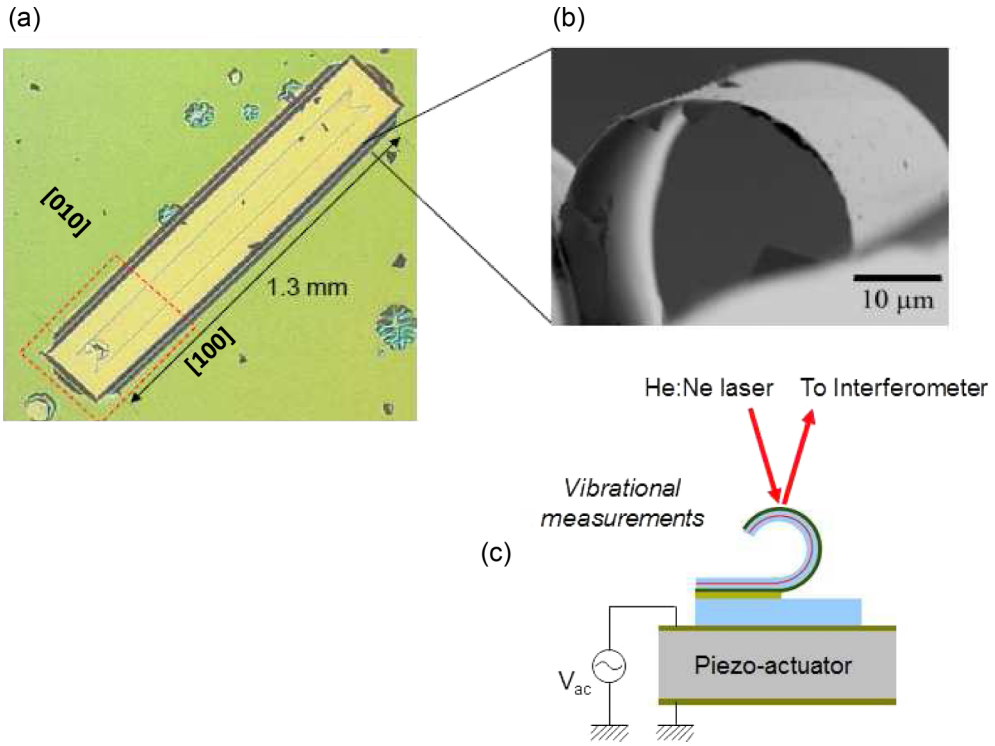

FIG. 1. (Color online) (a) Optical top view and (b) SEM image of an SRT. (c) Sketch of an SRT mounted on a piezocrystal.

using the GaAs material constants, the Young's modulus $E = 8.59\times10^{10}$ N/m^2, the Poisson ratio $\nu = 0.31$, and the density $\varrho = 5.32\times10^3$ kg/m^3. The shifts of the mode frequencies by rolling up a cantilever plate were already predicted by Izumida *et al.* [25]. The in- and out-of-plane motion in cantilevers are coupled, whereby in flat plates the in-plane strain strongly increases the frequencies of the main out-of-plane modes such as the bending and twisting modes. However, even for finite curvature, the out-of-plane modes may evade the in-plane extension, known as inextensionality. As a result, the bending modes follow a sixth-order differential equation including the curvature effect as an extension of the forth-order differential equation for the straight beam. Consequently, with a curvature, we find the following scaling functions on the pitch factor p:

$$f_1^{(b)}/f_1^{(0)} = 1 + 0.7872p^2 + 0.3698p^4,$$

$$f_2^{(b)}/f_1^{(0)} = 6.267 - 34.89p^2 + 80.61p^3 - 72.33p^4 + 23.89p^5.$$

The results of these scaling expressions were demonstrated in Fig. 2 of Ref. [25] as theoretical curves, although these expressions were not shown in Ref. [25]. Interestingly, the inextensionality for the excited bending mode leads to the opposite effect, a decrease of the frequency with curvature. We observe $f_2^{(b)} = 57.5$ kHz for our SRT, while $f_2^{(0)} = 105.9$ kHz is expected for the corresponding flat cantilever.

Surprisingly, we observe a significant splitting between the bending and twisting modes for both the ground and first exciting modes. Without any residual stress effects, we would expect only a little difference between the frequencies of the bending and twisting modes as shown by the dotted lines in the inset of Fig. 2. However, a significant shear strain $\gamma_{xy0} = Cx/l_x$ develops along the tube axis by relaxation of the layer during the detachment from the substrate. Then, the resulting residual shear stress $\tau_{x0} = c_{44}\gamma_{xy0}$ adds the term $U_{RS} = h\int dxdy\tau_{x0}(\partial w/\partial x)(\partial w/\partial y - v/r)$ to the strain energy of the tube, were ω and υ are the displacements along the circumference and normal to the SRT surface, respectively. For the calculations of the mode frequencies of with and without the residual stresses, we also take into account the cubic symmetry of GaAs, i.e., $c_{11} = 11.9\times10^{10}$ N/m^2, $c_{12} = 5.34\times10^{10}$ N/m^2, and $c_{44} = 5.96\times10^{10}$ N/m^2. We use the value $C = 4\times10^{-5}$. As a result, we estimate the splitting of the bending and twisting modes as shown in Fig. 2, which corresponds well with the experimental results. Note that the observed bending modes show small x dependence, that is the smaller amplitude near the edges. The calculated shapes for the bending modes also show the smaller amplitude near the edges which is induced by the residual shear strain. Finally, we note the significantly lower vibration amplitudes of the twisting modes as compared with the bending modes. This is the result of a selection rule due to the PZT excitation, which in general will not allow for any twisting modes, but only deviations from the tube perfection will lead to small twist vibration signals.

B. Electrical excitation and detection of the fundamental oscillations of rolled-up heterostructures

1. Bending modes of rolled-up heterostructure with weak inflection lines

We actuate the mechanical vibrations of the SRT by driving a current along the CP in a photolithographically defined electronic structure at temperature $T = 50$ mK. Similarly

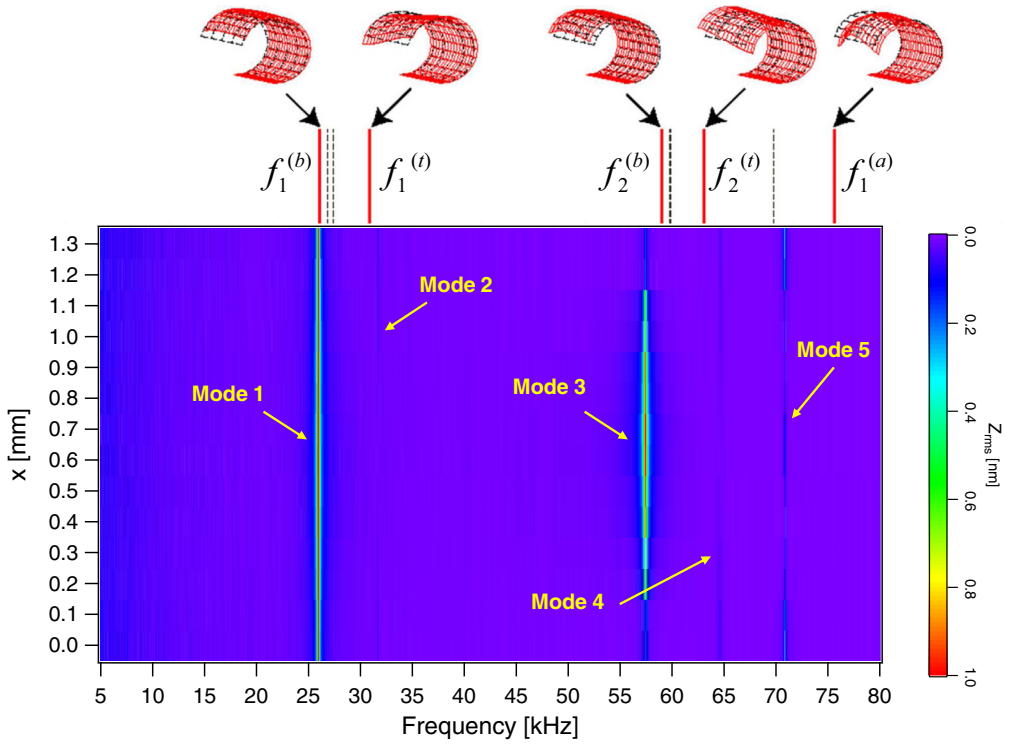

FIG. 2. (Color online) Amplitude of the mechanical vibrations z_{rms} as a function of the frequency and the position x along the axial direction. Interferometric measurements were carried out at room temperature and in vacuum. The inset on top of the graph shows the calculated frequencies and mode shapes for the ground and first excited bending modes $f_1^{(\mathrm{b})}$ and $f_2^{(\mathrm{b})}$, the ground and first excited twisting modes $f_1^{(\mathrm{t})}$ and $f_2^{(\mathrm{t})}$ and the axial mode $f_1^{(\mathrm{a})}$ as red lines. Animations of the vibrations are given in the Supplemental Material [26]. The dotted lines result of the calculations without taking into account the residual shear stress τ_{x0}.

to the optically detected vibration spectra and with similar amplitude relationships, we observe also seven modes in the frequency range below 200 kHz, as shown in Fig. 3 and listed in Table I. Note that both bending modes $f_1^{(\mathrm{b})}$ and $f_2^{(\mathrm{b})}$ and the ground twisting mode $f_1^{(\mathrm{t})}$ appear at even three times lower frequencies as compared to SRTs without photolithographically defined electronic structures. The strongest frequency decrease appears for the bending modes, where the main displacement takes place in the middle of

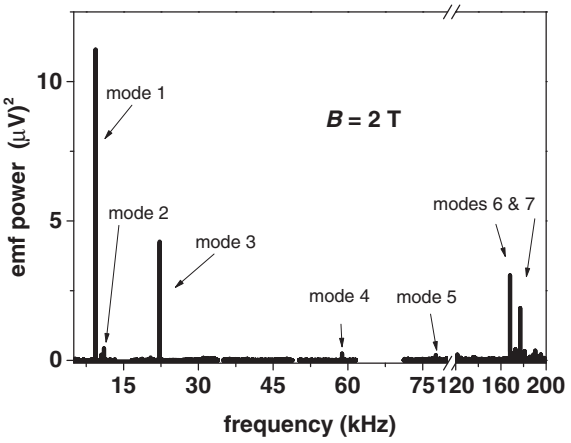

FIG. 3. Mechanical vibration modes in a SRT with $p = 0.73$ excited and detected by magnetomotive forces for $B = 2$ T at $T = 50$ mK.

the SRT, just in the region where the photolithographically defined electronic structure is located. The excited modes, for which the frequency decrease is less pronounced, exhibit the strongest vibration amplitude near the ends of the tube. Accordingly, we explain the frequency decrease of the bending modes by the different fabrication of the SRT for the electrical measurements, which includes a trench shallow etching to define the electronic structures. In our structures, there are three $b = 2$ μm wide trenches in the axial direction with an etching depth of about 60 nm, which is a significant part of the whole thickness of the SRT of 170 nm. Therefore the bending stress and strain within the trenches differs significantly from those values in the main part of the SRT, and we conclude that these trenches form weak inflection lines for the bending modes. Assuming that the main bending takes part within these inflection lines and taking into account the leverage effect of the remaining part of the cantilever, we expect an increased strain ε, resulting in a decrease of the average modulus $k = F/\varepsilon$ and therefore also the eigenfrequencies $f \sim k^{0.5}$. To prove it, we carried out model calculations by the two-dimensional finite-element-method (2DFEM) according to the schematic structure of the SRT presented in Fig. 4. In fact, this simple model results in decreased values $f_1^{(\mathrm{b})\mathrm{trench}} = 20.1$ kHz and $f_2^{(\mathrm{b})\mathrm{trench}} = 68.2$ kHz as compared with values of the trench-free SRT $f_1^{(\mathrm{b})} = 29.3$ kHz and $f_2^{(\mathrm{b})} = 74$ kHz, respectively. Although these calculations do not fully explain the frequency discrepancy, we believe that a more realistic model, which takes into account more specifically the real

TABLE I. Mode frequencies for the optical $f^{(i)}$(opt) and electrical $f^{(i)}$(el) detections, $r_1 = f^{(i)}(\text{el})/f^{(i)}(\text{opt})$, $r_p = f^{(i)}(p_1)/f^{(i)}(p_2)$.

mode (kHz)	$f_1^{(b)}$	$f_1^{(t)}$	$f_2^{(b)}$	$f_2^{(t)}$	$f_1^{(a)}$	$f_1^{(aw)}$	$f_2^{(aw)}$
optical detection, $p = 0.70$	26.0	31.5	57.5	64.0	71.8	168	186
electrical detection, $p_1 = 0.73$	9.45	11.06	22.16	59.00	78.25	168.0	172.8
electrical detection, $p_2 = 0.83$	7.59	9.61	17.13	52.95	74.00	125.1	137.0
r_1	0.36	0.35	0.39	0.92	1.09	1.00	0.93
r_p	1.27	1.12	1.29	1.13	1.06	1.35	1.26

electronic structure such as distributed trenches, may explain our observations.

The modes at even higher frequencies, including the axial and axial-wave motion should not be affected by the weak inflection lines that appear in the experiment. As expected, the mode frequencies generally decrease by increasing of the cantilever length l_y—expressed by the pitch factor of the SRT. In Table I, we provide also the ratio $r_p = f^{(i)}(p_1)/f^{(i)}(p_2)$ for two different pitch factors, p_1 and p_2. Their values for the bending modes are close to the expected ratio $(p_2/p_1)^2 = 1.29$ as predicted by the length dependence of the cantilever's frequency $f_1^{(0)} \sim 1/l_y^2$.

2. *Coupling of the high-mobility electron gas with the mechanical vibrations*

Figure 5 displays typical emf power spectra in two different magnetic fields as example of the ground bending mode. At temperatures as low as 50 mK and low magnetic fields, we observe resonance peaks with quality factors up to $Q = f/\delta f \approx 50\,000$, where f is the frequency at resonance and δf is the width at half maximum of the peak. By increasing the magnetic field, the resonances shift in frequency position and broaden significantly. In addition, the resonance power depends strongly on the excitation current and the angle with which the magnetic field penetrates the surface of the cylinder. We observe also an asymmetry of the resonance power with respect to the direction of the magnetic field.

The magnetic field dependence of the resonance spectra is typical for the magnetomotive effect, which was studied extensively for mechanical vibrations in MEMS and NEMS with a conducting gate [27,30,31]. In a magnetic field, the current $I(t)$ creates a Lorentz force $F(t) = lBI(t)$, which is directed perpendicular to the field and which results in a displacement $\Delta z(t)$. l is the length of the current path on the cantilever. The dynamics of the displacement itself creates an emf voltage $V_{\text{emf}}(t) = lB\ \mathrm{d}z/\mathrm{d}t$. For the SRT, the displacement velocity $\mathrm{d}z(t)/\mathrm{d}t$ should be recalculated in accordance with the velocity of the flux change through the loop area $S_{\text{CP}}(t) = l_{\text{CP}}z(t)$ penetrated by the magnetic field.

Both the excitation force and the resulting emf depend linearly on the corresponding magnetic field component. Therefore the resulting vibration reaction should be proportional to the square of the field. We prove this by measuring the vibration power A_{emf} for the ground bending mode at around 9 375 Hz in units of $(V_{\text{emf}}^{\max}/I_{\text{rms}})\delta f$ while rotating the SRT around the cylinder axis in the magnetic field. As shown in Fig. 6, for all rotation angles α, we find a clear linear dependence of A_{emf} on $B_{\parallel}$ in the double logarithmic representation corresponding to a quadratic magnetic field dependence. Consequently, the Lorentz force actuates the bending mode most effectively if it is directed perpendicular to the surface of the SRT.

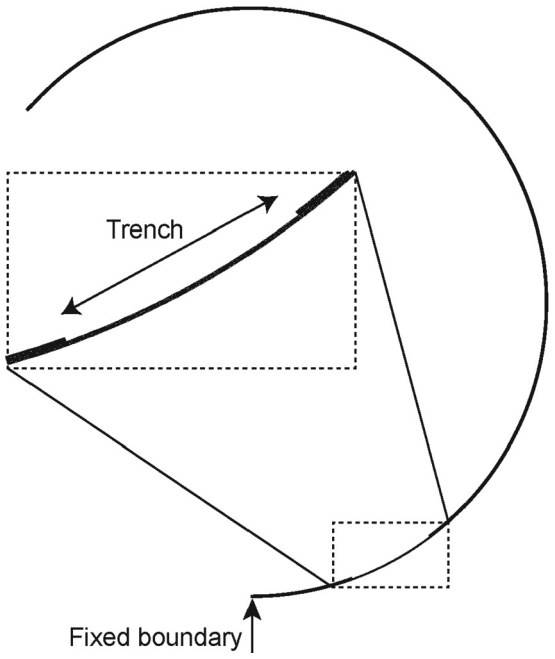

FIG. 4. Scheme of a SRT with a 80-μm-long and 0.2-μm-thick wall, containing a 6-μm-wide and 0.1-μm-deep trench as a weak link for the recalculation of the bending modes by using 2D finite element method with mesh $x = 2400$ and mesh $y = 10$.

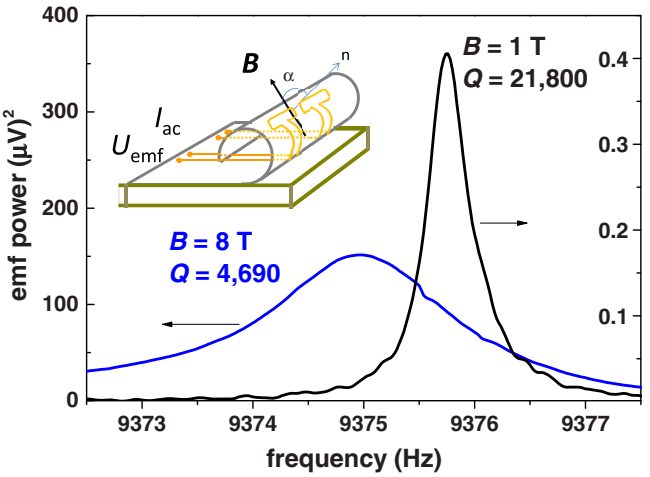

FIG. 5. (Color online) Emf power peak of the ground bending mode of an SRT for two different magnetic fields. The inset shows schematically the SRT with a conducting path.

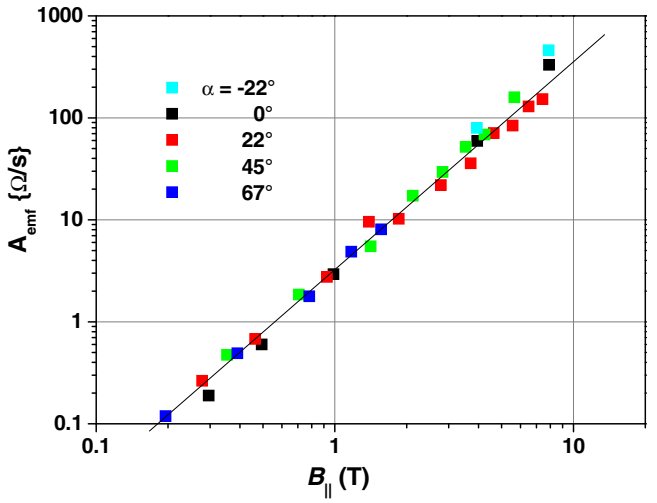

FIG. 6. (Color online) Vibration power $A_{\rm emf}$ as a function of $B_{\|}$ in the double logarithmic presentation for the ground bending mode at around 9 375 Hz for different rotation angles α. α starts from the angular position, where the magnetic field is directed perpendicular to the tube at the position of the CP with the exciting current. The line corresponds to the B^2 dependence with the proportionality factor $A_{\rm emf}/B_{\|}^2 \approx 3\ {\rm m}^2/{\rm kg}$. Measurements were carried out with exciting current $I_{\rm rms} = 150$ nA and at temperature $T = 50$ mK.

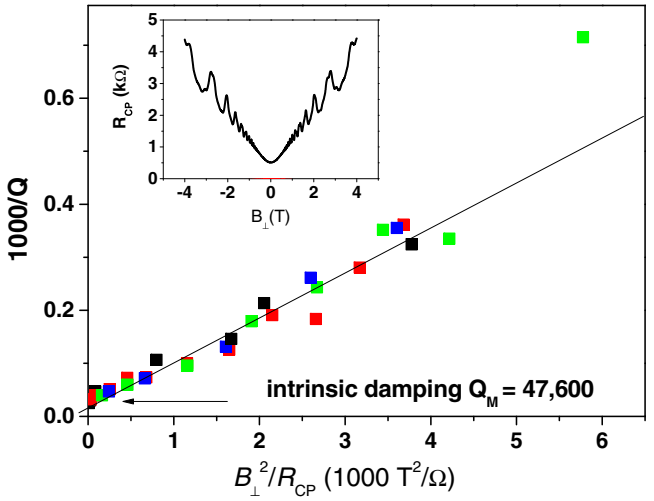

FIG. 7. (Color online) Quality factor $1000/Q$ of the ground bending mode as a function of $B_{\perp}^2/R_{\rm CP}$ for all rotation angles α as indicated in Fig. 6. The inset shows the two-terminal resistance at 13 Hz. The thin black line is a guide to the eyes. The intercept with the y axis gives the intrinsic mechanical quality factor $Q_M = 47\,600$. Measurements were carried out with exciting current $I_{\rm rms} = 150$ nA and at temperature $T = 50$ mK.

Mechanical vibrations due to magnetomotive forces are highly sensitive to dissipation processes due to parasitic components in the electronic circuitry and Eddy currents, which arise in addition to the driving current and which oppose the driving force. Therefore the inverse quality factor is the sum of the intrinsic mechanical losses described by the quality factor $1/Q_M$ of the SRT and the electronic damping part in its general expression [27,32] according to

$$\frac{1}{Q} = \frac{1}{Q_M} + \frac{B_{\perp}^2 l^2}{m 2\pi f |Z|}. \qquad (1)$$

The impedance $|Z|$ includes electronic losses due to embedding in the external circuit especially for high frequencies. For the Eddy current losses, $|Z|$ may be expressed by the loop resistance $R_{\rm CP}$ [30], which for HM2DEG in SRTs depends strongly on the perpendicular to the CP directed magnetic field component $B_{\perp}$. We show the two-terminal loop resistance $R_{\rm CP}$ measured at 13 Hz in the inset of Fig. 7. Due to the strong dependence of $R_{\rm CP}$ on $B_{\perp}$, we compile the experimental inverse quality factor $1/Q$ data from all rotation angles in one common plot, using $B_{\perp}^2/R_{\rm CP}$, see Fig. 7. We find an excellent agreement with Eq. (1) for the lowest frequency mode despite some scatter of the data mainly due to the Shubnikov-de Haas oscillations in $R_{\rm CD}$. The intersect with the y axis gives the value for the intrinsic quality factor $Q_M \approx 47\,600$, while the slope of the electronic part of the losses allows to estimate a ratio $l^2/m \approx 5070\ {\rm m}^2/{\rm kg}$.

With the mass of the SRT $m \approx 1\times10^{-10}$ kg, we estimate a length $l \approx 710\ \mu$m, which is close to the value of the actual length of the current path $l_{\rm CD} = 600\ \mu$m on the SRT. Therefore we conclude that Eddy currents are the main damping sources for the lowest frequency modes. The slightly longer value of l arises from some external electronic impedance, which becomes more important for modes at higher frequencies. It is well known that also the frequency of the modes varies with dissipation [27,32]. This comprises the coupling between the mechanical vibration and the HM2DEG. Figure 8 shows the emf power of the vibration as a function of the frequency and the magnetic field, which reflects the electronic properties of the HM2DEG. We clearly observe Shubnikov-de Haas

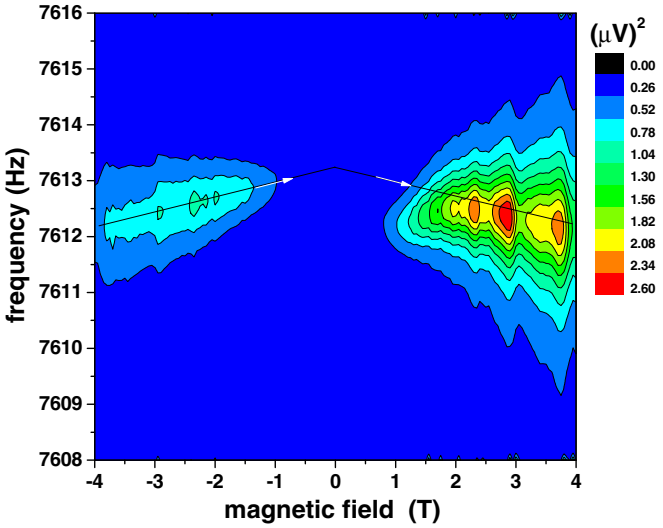

FIG. 8. (Color online) Emf power of the ground bending mode for the SRT with $p = 0.83$ as a function of the magnetic field and frequency. Mechanical vibrations are excited by a current of 150 nA at $T = 50$ mK. The thin black lines are guides to the eye. The arrows show the present sweep direction of the magnetic field. The lower frequency values at low positive magnetic fields as compared to its negative counterparts uncover a hysteresis behavior.

oscillations (SdH) and the quantum Hall effect (QHE). For the low-frequency modes, we observe generally a reduction of the resonance frequency, called mode softening, while for the high-frequency modes, we observe often a stiffening while increasing the magnetic field. The reason for this is unknown yet. A detailed analysis shows, that SdH and QHE appear also in the linewidth as well as in the frequency position through the dissipation by R_{CP}. Figure 8 displays also a hysteresis behavior around low fields. While sweeping the magnetic fields from negative to positive values, the resonance frequencies at positive low magnetic fields are lower as the ones at negative fields and vice versa. One reason may be, that the temperature in the mixing chamber increases suddenly by switching the magnetic field direction. As a result, at temperatures below 1 K, the strong temperature dependencies of Q and f_0 may uncover a slow velocity of the system recovery to equilibrium, even at sweep rates below 10 mT/min. In addition, we observe a prominent asymmetry in the vibration power and the coupling with respect to the directions of the magnetic field. The magnetic field asymmetry is a general property of the HM2DEG on curved surfaces due to the broken symmetry. In particular, for transport properties, by placing a tube with a high mobility 2DEG in a static and homogeneous magnetic field B_0, a fundamental dominant modification is the gradual change of the component of the magnetic field perpendicular to the surface $B_\perp$ along the periphery of the tube, which is equivalent to a gradual change of the filling factor ν. Then, as shown previously [8,11,33], any current flow, therefore also the flow of the Eddy currents will redistribute on the curved surface differently for different magnetic field directions. Our results in Fig. 8 clearly show the impact of the properties of the curved HM2DEG on the mechanical-electrical coupling.

IV. CONCLUSION

We observed vibration modes in SRTs and found an excellent agreement with the theoretically calculated frequencies for the ground bending and excited bending as well as axial modes. The effect of the curvature is to increase the frequencies of the ground bending modes and the axial wave modes, while the frequency for the excited bending mode decreases. We find an unexpected and significant splitting of the bending and twisting modes, which originates from residual stress effects due to axial shear relaxation in z-dependent modes. We are able to excite and detect the vibration modes also by means of electronic structures, which are fabricated via trench etching into the thin tube walls. Mechanically, these trenches form weak inflection lines which result in a drastic decrease of the eigenfrequencies of the bending modes. The high-mobility electrons interact with the mechanical motion due to Eddy currents and embedded impedances, which decreases the quality factor and leads to mode shifting in magnetic fields. In addition, we observe a prominent asymmetry in the mechanical-electrical coupling in a homogeneous magnetic field, which originates from the broken symmetry of HM2DEG on curved surfaces.

ACKNOWLEDGMENTS

The authors gratefully acknowledge stimulating discussions with P. Santos and H.T. Grahn. We thank M. Höricke and A. Buchholz for technical assistance. This work was supported in part by the DFG-JST Strategic Japanese-German Cooperative Program on “Nanoelectronics” (Nos. FR 930/16-1 and AOBJ 548229). We acknowledge JSPS KAKENHI Grant Nos. 22740191 and 23241046, Japan.

[1] V. Y. Prinz, V. A. Seleznev, A. K. Gutakovsky, A. V. Chehovskiy, V. V. Preobrazhenskii, M. A. Putyato, and T. A. Gavrilova, Physica E (Amsterdam) **6**, 828 (2000).
[2] V. Y. Prinz, V. A. Seleznev, A. V. Prinz, and A. V. Kopylov, Sci. Technol. Adv. Mater. **10**, 034502 (2009).
[3] F. Li, Z. Mi, and S. Vicknesh, Opt. Lett. **34**, 2915 (2009).
[4] X. Li, J. Phys. D: Appl. Phys. **41**, 193001 (2008).
[5] D. Grimm, C. C. B. Bufon, C. Deneke, P. Atkinson, D. J. Thurmer, F. Schäffel, S. Gorantla, A. Bachmatiuk, and O. G. Schmidt, Nano Lett. **13**, 213 (2013).
[6] K. Jensen, K. Kim, and A. Zettl, Nat. Nanotechnol. **3**, 533 (2008).
[7] K.-J. Friedland, A. Riedel, H. Kostial, M. Höricke, R. Hey, and K.-H. Ploog, J. Electron. Mat. **30**, 817 (2001).
[8] K.-J. Friedland, R. Hey, H. Kostial, A. Riedel, and K. H. Ploog, Phys. Rev. B **75**, 045347 (2007).
[9] A. B. Vorob’ev, K.-J. Friedland, H. Kostial, R. Hey, U. Jahn, E. Wiebicke, J. S. Yukecheva, and V. Y. Prinz, Phys. Rev. B **75**, 205309 (2007).
[10] K.-J. Friedland, R. Hey, H. Kostial, and A. Riedel, Phys. Status Solidi C **5**, 2850 (2008).
[11] K.-J. Friedland, A. Siddiki, R. Hey, H. Kostial, A. Riedel, and D. K. Maude, Phys. Rev. B **79**, 125320 (2009).
[12] H. Yamaguchi, Y. Tokura, S. Miyashia, and Y. Hirayama, Phys. Rev. Lett. **93**, 036603 (2004).
[13] N. Lambert, I. Mahboob, M. Pioro-Ladri‘ere, Y. Tokura, S. Tarucha, and H. Yamaguchi, Phys. Rev. Lett. **100**, 136802 (2008).
[14] J. P. Eisenstein, H. L. Stormer, V. Narayanamurti, A. Y. Cho, A. C. Gossard, and C. W. Tu, Phys. Rev. Lett. **55**, 875 (1985).
[15] J. G. E. Harris, R. Knobel, K. D. Maranowski, A. C. Gossard, N. Samarth, and D. D. Awschalom, Phys. Rev. Lett. **86**, 4644 (2001).
[16] N. Ruhe, G. Stracke, C. Heyn, D. Heitmann, H. Hardtdegen, T. Schäpers, B. Rupprecht, M. A. Wilde, and D. Grundler, Phys. Rev. B **80**, 115336 (2009).
[17] A. Naik, O. Buu, M. D. LaHaye, A. D. Armour, A. A. Clerk, M. P. Blencowe, and K. C. Schwab, Nature (London) **443**, 193 (2006).
[18] A. D. O′Connell, M. Hofheinz, M. Ansmann, R. C. Bialczak, M. Lenander, E. Lucero, M. Neeley, D. Sank, H. Wang, M. Weides, J. Wenner, J. M. Martinis, and A. N. Cleland, Nature (London) **464**, 697 (2010).

[19] I. Mahboob, K. Nishiguchi, H. Okamoto, and H. Yamaguchi, Nat. Phys. **8**, 387 (2012).
[20] H. Okamoto, A. Gourgout, C.-Y. Chang, K. Onomitsu, I. Mahboob, E. Y. Changand, and H. Yamaguchi, Nat. Phys. **9**, 480 (2013).
[21] I. Mahboob, K. Nishiguchi, A. Fujiwara, and H. Yamaguchi, Phys. Rev. Lett. **110**, 127202 (2013).
[22] H. Yamaguchi and I. Mahboob, New J. Phys. **15**, 015023 (2013).
[23] J. Stettenheim, M. Thalakulam, F. Pan, M. Bal, Z. Ji, W. Xue, L. Pfeiffer, K. W. West, M. P. Blencowe, and A. J. Rimberg, Nature (London) **466**, 86 (2010).
[24] H. Okamoto, D. Ito, K. Onomitsu, H. Sanada, H. Gotoh, T. Sogawa, and H. Yamaguchi, Phys. Rev. Lett. **106**, 036801 (2011).
[25] W. Izumida, Y. Hirayama, H. Okamoto, H. Yamaguchi, and K.-J. Friedland, Phys. Rev. B **85**, 075313 (2012).
[26] See Supplemental Material at http://link.aps.org/supplemental/10.1103/PhysRevB.89.245304 for animation of the vibrations.
[27] A. N. Cleland and M. L. Roukes, Sens. Actuators, A **72**, 256 (1999).
[28] H. Yamaguchi, H. Okamoto, Y. Maruta, S. Ishihara, S. Miyashita, and Y. Hirayama, Jpn. J. Appl. Phys. **46**, L658 (2007).
[29] H. Yamaguchi, H. Okamoto, S. Ishihara, and Y. Hirayama, Appl. Phys. Lett. **100**, 012106 (2012).
[30] X. M. H. Huang, X. L. Feng, C. A. Zorman, M. Mehregany, and M. L. Roukes, New J. Phys. **7**, 247 (2005).
[31] K. L. Ekinci and M. L. Roukes, Rev. Sci. Instrum. **76**, 061101 (2005).
[32] K. Schwab, Appl. Phys. Lett. **80**, 1276 (2002).
[33] A. V. Chaplik, JETP Lett. **72**, 503 (2000).